ASIAN JOURNAL OF CIVIL ENGINEERING (BUILDING AND HOUSING) VOL. 10, NO. 4 (2009)
PAGES 361-380

MODELING TRANSIENT ELASTODYNAMIC PROBLEMS USING SPECTRAL ELEMENT METHOD

N. Khaji*, M. Habibi and P. Mirhashemian
Department of Civil Engineering, Tarbiat Modares University, Tehran, Iran

ABSTRACT

This study investigates a time-domain method for modeling general transient elastodynamic problems using the spectral-based finite element method (SEM) which is based upon a conforming mesh of two-dimensional quadrilaterals. Employing the Galerkin weighted residual method, detailed formulation of the SEM is derived in which various aspects involving in elastodynamic problems are discussed. The accuracy and efficiency of the method is fully demonstrated by comparing results obtained from the SEM with those reported in other studies. For this purpose, a set of wave propagation and structural dynamic problems, subjected to various load forms such as triangular load, Heaviside step load, sinusoidal impulsive load, and ramped load are modeled using the SEM. Furthermore, support motion boundary conditions are examined using the SEM. Each problem is successfully modeled using a very small number of degrees of freedom in comparison with other numerical methods. The numerical results agree very well with the analytical solutions as well the results from other numerical methods.

Keywords: Spectral element method; finite element method; elastodynamics; dynamic analysis

1. INTRODUCTION

Elastodynamics illustrates a broad range of phenomena in engineering and physical problems such as fluid-structure interaction [1] and soil-structure interaction [2] in which, general form of wave equations (in fluid and solid domains) with suitable boundary conditions (BCs) should be solved. Coming along with the huge increase of computational capacities, numerical methods have provided robust and effective forums to challenge wave propagation phenomenon during the last three decades, among which finite difference method (FDM) [3], boundary element method (BEM) [4-7], and finite element method (FEM) [8-10] are most popular. Spectral-based finite element method (SEM) provides a high-order technique which, therefore, allows obtaining the same accuracy as low-order

* Email-address of the corresponding author: nkhaji@modares.ac.ir (N. Khaji)

methods (such as FEM and FDM) by using a reduced number of grid points, thus giving rise to a significant efficiency in computational resources. The SEM which uses all the advantages of the classical FEM (e.g., well-suited to handle complex geometries and interface conditions), has been benefited by special sort of interpolation functions which, on our knowledge, are being somehow similar to fundamental solutions employed in the BEM. These interpolation functions enable the SEM to transfer a wide range of wavelengths through elements with higher accuracy and lower computational efforts comparing to the classical FEM. In other words, each spectral element could be imagined as a small domain modeled by a simplified BEM in which, by 'simplified' we mean a simple fashion of fundamental solutions which involves no singular integrals to be computed. The SEM which was originally introduced in computational fluid mechanics [11] is currently being implemented in structural- [12-14] and continuum- [15,16] based elastodynamics problems.

Various features of the SEM as a time-domain approach for general transient elastodynamic analyses are inspected in the present work. The SEM approach is based on the following idea. First, the computational domain is decomposed into quadrilateral non-overlapping subdomains/elements. Then, the solution is expressed as a truncated expansion of a tensor product of Legendre orthogonal polynomials on each subdomain. Following the Galerkin formulation [17], the semi-discrete formulation of the wave equation is then written. This is formally represented by a system of linear, second-order, ordinary differential equations, which must be integrated in time. In this last step, the semi-discrete equation is solved by assembling the global system matrices and integrating numerically the resulting ordinary differential equations [18].

Finally, a set of wave propagation and structural dynamics problems, subjected to various transient load forms, are modeled to validate the present approach.

Since this method shows a promising performance in solving problems in which elastic wave propagation plays an important role, development of this approach for large-scale three-dimensional seismic wave propagation in real engineering seismology problems is currently followed by the authors.

2. GOVERNING EQUATIONS

The following presentation is restricted to the isotropic, homogeneous, small-displacement linear elastic behavior. The equations of motion that govern the propagation of elastic waves in a solid may be solved based upon either a strong or a weak formulation of the problem. In the strong formulation one works directly with the equations of motion and associated boundary conditions written in differential form. In the weak formulation, one uses an integral form of the equations of motion, as in the FEM [17]. The SEM is based upon a weak formulation of the equations of motion.

The equilibrium equations for an elastic bounded medium $\Omega \subset \mathbb{R}^d$ (d = 2, 3 is the number of space dimensions), subjected to an external body-force f_i is described by

$$\sigma_{ij,j} + f_i = \rho \ddot{u}_i \quad , \quad i = 1,...,d \tag{1}$$

where $\ddot{u}_i = \partial^2 u_i / \partial t^2$ is the second derivative of displacement of the medium with respect to time; ρ, the mass density, and σ_{ij} denotes the stress tensor components.

Instead of using the equations of motion and associated BCs directly, strong form as in Eq. (1), one can use an integrated form (i.e., weak form such as weighted residual approach). This is accomplished by weighting Eq. (1) with an arbitrary test vector (the variation of displacement function is chosen here), integrating by parts over the model volume Ω, and imposing suitable BCs. This gives

$$\int_{\Omega} \delta u_i (\sigma_{ij,j} + f_i - \rho \ddot{u}_i) d\Omega = 0 \tag{2}$$

or

$$\int_{\Omega} \delta u_i \sigma_{ij,j} d\Omega + \int_{\Omega} \delta u_i f_i d\Omega - \int_{\Omega} \delta u_i \rho \ddot{u}_i d\Omega = 0 \tag{3}$$

The first integral of Eq. (3) can now be integrated by parts (Green's Lemma) to obtain the weak form as below

$$\int_{\Omega} \delta u_i \sigma_{ij,j} d\Omega = \int_{\Gamma} \delta u_i \sigma_{ij} n_j d\Gamma - \int_{\Omega} (\delta u_i)_{,j} \sigma_{ij} d\Omega \tag{4}$$

in which Γ is the boundary of the physical domain Ω, and n_j denotes the jth component of the outward unit vector orthogonal to the boundary. Two variational and differential operators are commutative thus provide

$$\int_{\Omega} \delta u_i \sigma_{ij,j} d\Omega = \int_{\Gamma} \delta u_i \sigma_{ij} n_j d\Gamma - \int_{\Omega} \delta u_{i,j} \sigma_{ij} d\Omega \tag{5}$$

or

$$\int_{\Omega} \delta u_i \sigma_{ij,j} d\Omega = \int_{\Gamma} \delta u_i t_i d\Gamma - \int_{\Omega} \delta \varepsilon_{ij} \sigma_{ij} d\Omega \tag{6}$$

where t_i and ε_{ij} are the traction components on Γ and the strain tensor components, respectively.

Considering Eq. (6), Eq. (3) could be written as

$$-\int_{\Omega} \delta \vec{\varepsilon}^T \vec{\sigma} d\Omega + \int_{\Gamma} \delta \vec{u}^T \vec{t} d\Gamma + \int_{\Omega} \delta \vec{u}^T \vec{f} d\Omega - \int_{\Omega} \delta \vec{u}^T \rho \ddot{\vec{u}} d\Omega = 0 \tag{7}$$

which shall be followed in Section 4.

3. MESH DEFINITION

A spectral element approximation of Eq. (2) and its solution are obtained as follows. First, the domain Ω is decomposed into n_e quadrilateral (2D) non-overlapping elements Ω_e, e = 1, ..., n_e, such that $\Omega = \bigcup_e^{n_e} \Omega_e$. Second, an expansion in terms of a tensor-product of Nth-order

orthogonal polynomials is used to approximate solution, data, geometry and physical properties on each element. Each quadrilateral spectral element is analogous to the square; hence, we adopt a suitable mapping between the square (master/reference element) and each spectral element Ω_e [17]. The master square is defined in terms of (ξ,η), $-1\le\xi\le1$, $-1\le\eta\le1$, which are sometimes referred to as the initial coordinates. Each quadrilateral element Ω_e is defined in terms of a set of n_a shape functions $N_a(\xi, \eta)$, $a = 1, ..., n_a$. For any given quadrilateral element, the relation between a point $\vec{x}$ within the element and a point (ξ, η) in the master square may thus be written in the form

$$\vec{x}(\xi,\eta)=\sum_{a=1}^{n_a}N_a(\xi,\eta)\vec{x}_a \tag{8}$$

in which, the shape functions $N_a(\xi, \eta)$ are products of Lagrange polynomials. The $(n_\ell+1)$Lagrange polynomials of degree$!n_\ell$ are defined in terms of $(n_\ell+1)$ control points $-1\le\xi_p\le1$, $p=0,...,n_\ell$, by

$$h_p^{n_\ell}(\xi)=\frac{(\xi-\xi_0)\cdots(\xi-\xi_{p-1})(\xi-\xi_{p+1})\cdots(\xi-\xi_{n_\ell})}{(\xi_p-\xi_0)\cdots(\xi_p-\xi_{p-1})(\xi_p-\xi_{p+1})\cdots(\xi_p-\xi_{n_\ell})}=\prod_{\substack{i=0\\ i\neq p}}^{n_\ell}\frac{(\xi-\xi_i)}{(\xi_p-\xi_i)} \tag{9}$$

In what follows, two-dimensional formulation is presented and discussed. A differential element of area *dxdy* within a given quadrilateral element Ω_e is related to a differential element of area $d\xi\, d\eta$ in the master square by

$$dxdy = J_e\, d\xi\, d\eta \tag{10}$$

where J_e denotes the Jacobian of the transformation

$$J_e=\left\|\frac{\partial\vec{x}}{\partial\xi}\times\frac{\partial\vec{x}}{\partial\eta}\right\|. \tag{11}$$

To calculate the Jacobian J_e one needs to determine the partial derivatives of Eq. (11). This is accomplished by differentiating the mapping Eq. (8)

$$\frac{\partial x(\xi,\eta)}{\partial\xi}=\sum_{a=1}^{n_a}\frac{\partial N_a(\xi,\eta)}{\partial\xi}x_a,\ \frac{\partial x(\xi,\eta)}{\partial\eta}=\sum_{a=1}^{n_a}\frac{\partial N_a(\xi,\eta)}{\partial\eta}x_a,\ \frac{\partial y(\xi,\eta)}{\partial\xi}=\sum_{a=1}^{n_a}\frac{\partial N_a(\xi,\eta)}{\partial\xi}y_a,$$
$$\frac{\partial y(\xi,\eta)}{\partial\eta}=\sum_{a=1}^{n_a}\frac{\partial N_a(\xi,\eta)}{\partial\eta}y_a \tag{12}$$

4. REPRESENTATION OF WEAK FORM ON THE MESH

To solve the weak form of the governing equations given in Eq. (7), integrations over the volume Ω and the boundary Γ are subdivided in terms of smaller integrals over the volume

and surface elements Ω_e and Γ_e, respectively

$$-\int_{\Omega_e}\delta\vec{\varepsilon}^T\vec{\sigma}d\Omega+\int_{\Gamma_e}\delta\vec{u}^T\vec{t}\,d\Gamma+\int_{\Omega_e}\delta\vec{u}^T\vec{f}d\Omega-\int_{\Omega_e}\delta\vec{u}^T\rho\ddot{\vec{u}}d\Omega=0 \tag{13}$$

As shown in the previous section, the shape of the quadrilateral elements can be defined in terms of low-degree Lagrange polynomials. In the FEM, low-degree polynomials are also used as basis functions for the representation of fields on the elements (which is a so-called isoparametric formulation).

For reasons discussed in the next sections, the control points ξ_p, $p=0,...,n_\ell$, needed in the definition (9) of the Lagrange polynomials of degree n_ℓ are placed at special positions called Legendre-Gauss-Lobatto (LGL) points. These correspond, in a normalized 1D situation (interval [-1, 1]), to the zeroes of P'_{n_ℓ}, the derivative of the Legendre polynomial of degree n_ℓ, and the extremes of the interval

$$\{\text{zeros of } P'_{n_\ell}(\xi)\}\cup\{\text{-1, 1}\} \tag{14}$$

which means that one has $(n_\ell+1)$ LGL points for a polynomial of degree n_ℓ.

On each elements Ω_e, a function f is interpolated by products of Lagrange polynomials of degree n_ℓ as

$$f(\vec{x}(\xi,\eta))\approx\sum_{a=1}^{n_e}N_a(\xi,\eta)f_a=\sum_{p=0}^{n_\ell}\sum_{q=0}^{n_\ell}h_p(\xi)h_q(\eta)f_{pq} \tag{15}$$

where the coefficients f_{pq} are the functional values of f at the interpolation points! $\vec{x}(\xi_p,\eta_q)$

$$f_{pq}=f(\vec{x}(\xi_p,\eta_q)) \tag{16}$$

In a similar fashion of Eq. (8), orthogonal polynomials (or interpolation functions) are used as basis functions for the representation of field quantities, say displacement components $\vec{u}$, on the elements Ω_e in a matrix form as follows

$$\vec{u}=[N]\vec{a} \tag{17}$$

in which the components of $[N]$ are interpolation functions, and $\vec{a}$ represents a listing of nodal displacements for a particular element Ω_e. The variation of displacement function is

$$\delta\vec{u}=[N]\delta\vec{a} \tag{18}$$

Strain tensor is defined in terms of the displacements by the well-known relations which

define the operator $[L]$

$$\vec{\varepsilon} = [L]\vec{u} \quad , \quad [L] = \begin{bmatrix} \partial/\partial x & 0 & \partial/\partial y \\ 0 & \partial/\partial y & \partial/\partial x \end{bmatrix}^T \tag{19}$$

Combining Eqs. (17)-(19) results in

$$\vec{\varepsilon} = [B]\vec{a} \quad , \quad [B] = [L][N] \tag{20}$$

and

$$\delta\vec{\varepsilon} = [B]\delta\vec{a} \tag{21}$$

in which $[B]$ is the well-known strain-displacement transformation matrix.

The stress tensor is linearly related to the strain tensor by Hooke's law, which in an elastic, isotropic solid may be written in the form of

$$\vec{\sigma} = [C]\vec{\varepsilon} \tag{22}$$

or

$$\vec{\sigma} = [C][B]\vec{a} \tag{23}$$

Substituting Eqs. (18), (21) and (23) in Eq. (13) and some algebraic manipulations, Eq. (13) may lead to a system of second-order ordinary differential equations in time

$$[M^e]\ddot{\vec{a}} + [K^e]\vec{a} + \vec{F}_t^e + \vec{F}_{ext.}^e = \vec{0} \tag{24}$$

where $[M^e]$ and $[K^e]$ are the mass matrix and stiffness matrices, respectively, at the element level; $\vec{F}_t^e$ and $\vec{F}_{ext.}^e$ are the local discrete representations of the forcing terms for external traction and body-force, respectively, at the element level

$$[M^e] = \int_{\Omega_e} \rho [N]^T [N] d\Omega \tag{25}$$

$$[K^e] = \int_{\Omega_e} [B]^T [C][B] d\Omega \tag{26}$$

$$\vec{F}_t^e = -\int_{\Gamma_e} [N]^T \vec{t}\, d\Gamma \tag{27}$$

$$\vec{F}_{ext.}^e = -\int_{\Omega_e} [N]^T \vec{f} d\Omega \,. \tag{28}$$

The $[M]$ and $[K]$ global matrices are the discrete counterparts of the integrals over the domain Ω and are equivalent to the sum of integrals over the set of the elements Ω_e of the partition. They are built through the assembly process of the element matrices (direct

stiffness method). The $[M]$ and $[K]$ system matrices and the forcing terms vector are given by

$$[M]=\sum_{e=1}^{n_e}[M^e] \quad , \quad [K]=\sum_{e=1}^{n_e}[K^e] \quad , \quad \vec{F}_t=\sum_{e=1}^{n_e}\vec{F}_t^{\,e} \quad , \quad \vec{F}_{ext.}=\sum_{e=1}^{n_e}\vec{F}_{ext.}^{\,e} \tag{29}$$

As a result, the system of equations (24) poses the global level form as

$$[M]\ddot{\vec{a}}+[K]\vec{a}+\vec{F}_t+\vec{F}_{ext.}=\vec{0} \tag{30}$$

4.1 Numerical integration of element matrices

The integrals of characteristics matrices being appeared in Eqs. (25)-(28) are usually calculated by Gauss quadrature in the FEM. In the SEM, integrations over the elements Ω_e may be approximated using the Legendre-Gauss-Lobatto (LGL) quadrature rule instead,

$$\int_{\Omega_e} f(\vec{x})dxdy=\int_{-1}^{1}\int_{-1}^{1} f(\vec{x}(\xi,\eta))J_e(\xi,\eta)d\xi d\eta \approx \sum_{p,q=0}^{n_\ell}\omega_p\omega_q f_{pq}J_{e(pq)} \tag{31}$$

in which ω_p and ω_q are the weights associated with the LGL points of integration, and $J_{e(pq)}=J_e(\xi_p,\eta_q)$.

To integrate the functions and their partial derivatives over the elements, the values of the inverse Jacobian matrix $\partial\vec{\xi}/\partial\vec{x}$ need to be determined at the $(n_\ell+1)^2$ LGL integration points for each element.

A highly interesting property of the SEM is the fact that the mass matrix $[M]$ is diagonal [16] thanks to using LGL quadrature for each element. This allows for a very significant reduction in computational cost and complexity, and thus, no costly linear system resolution algorithm is needed to march the system in time.

4.2 Time integration of the global system

The system of ordinary differential equations (30) that governs the time dependence of the global system may be written in the form of

$$[M]\ddot{\vec{a}}+[K]\vec{a}=\vec{F} \tag{32}$$

where $\vec{F}$ indicate the source term. The system of equations (32) is integrated in time by various schemes [17]. In this research, time discretization of Eq. (32) is achieved based upon a classical central-difference scheme, moving the stiffness term to the right-hand side. Since this scheme is fully explicit and conditionally stable, in order to ensure stability, it must satisfy the usual Courant-Friedrichs-Levy (CFL) condition. The Courant stability number of the explicit time integration schemes is defined as

$$C=\Delta t\left(\frac{c}{\Delta h}\right)_{\max} \tag{33}$$

in which, Δh is the minimum grid spacing, c the maximum propagation velocity of stress waves and Δt denotes the time step chosen. The CFL condition [15] states that C should not be chosen higher than an upper limit

$$C \le C_{\max} \tag{34}$$

For most practical purposes and regular meshes, the value $C_{\max} = 0.5$ is acceptable, while for very irregular meshes with distorted elements the upper limit reduces to approximately 0.3 to 0.4. For a given element, using higher-order interpolation functions decreases Δh, resulting in smaller Δt to be selected (see Eq. (33)). In these cases, the Courant stability condition may be too restrictive for an explicit scheme. In that case, a Newmark scheme as an implicit one can be used instead.

4.3 Interpolation functions and mesh considerations

In the SEM as other typical mesh-based numerical methods, spatial resolution is controlled by the typical size of an element, and the polynomial degree used to represent interpolation functions on an element, n_ℓ. If the polynomial degree n_ℓ is too small (e.g. less than typically 4), the SEM shows the same inaccuracies that are observed in the FEM applied to wave propagation problems [19]. A very large (e.g. greater than 15) degree of the polynomial on the other hand, makes the method spatially very accurate, but the computational costs become huge. In the SEM for wave propagation problems one typically uses a polynomial degree between 5 and 10 to provide the best balance between accuracy and cost. To obtain accurate results, Δh has to be chosen such that the average number of points per minimum wavelength ($\lambda_{\min} = (n_\ell + 1)\Delta h$) in an element, is roughly equal to 5 for the optimal range of polynomial degrees ($5 \le n_\ell \le 10$) [18].

For the design of the mesh as in the FEM, the curvature of the elements should be modest, such that the Jacobian of the mapping to the reference domain varies smoothly across any given element and never vanishes [17].

5. NUMERICAL EXAMPLES

The aforementioned methodology has been implemented in a two-dimensional time-domain SEM code in which, a library of spectral quadrilateral elements with various orders is provided. In order to validate the nature and general behavior of the method, five numerical examples have been considered. A plane stress condition is assumed for all the examples. Numerical results are compared with those obtained by exact analytical solutions [20] and/or by other numerical methods to assess the stability and the accuracy of the present method. No physical damping (i.e., pure elastic material behavior) is considered in all the SEM analyses. All quantities are measured in SI units.

5.1 Rectangular bar subjected to two different loadings

In the first example, verification of the algorithm especially in comparison with analytical solutions is the main target. A rectangular bar (see Figure 1a), whose length L is twice its width W, is fixed at its left end with traction free on its top and bottom sides. The Poisson's ratio is considered null to impose one-dimensional condition. The right end side of bar is uniformly subjected to two various tensile loadings: a Heaviside step function representing a suddenly applied load (P_0 = 1) as shown in Figure 1b, and a triangular function which increases from zero at time t = 0 to P_0 at t = 1, and then decreases to zero at t = 2 as depicted in Figure 1c. The material constants are as follows: the Young's modulus E = 1, and the mass density ρ = 1. These material properties yield the maximum propagation velocity of stress waves c = 1. In the triangular loading, the primary wave front just reaches the fixed end at time t = 1, and bounces back to the right end at t = 2.

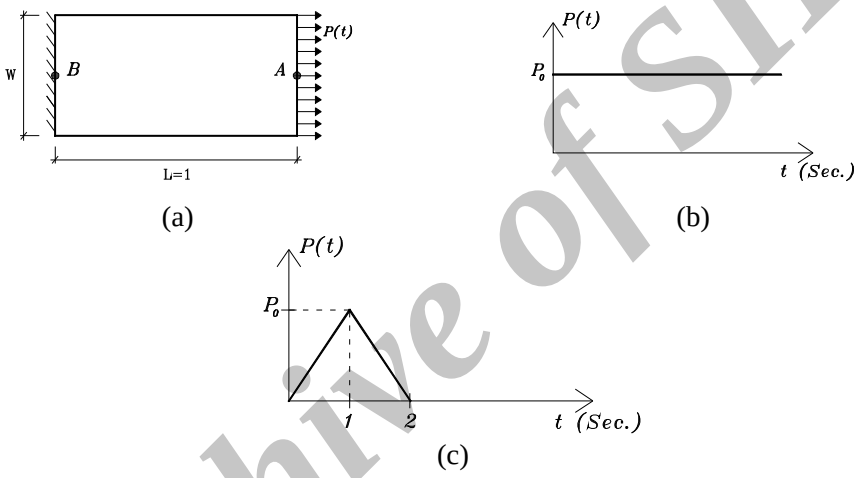

Figure 1. The first example. Rectangular bar subjected to prescribed loading: (a) geometry and boundary conditions, (b) Heaviside loading, (c) triangular loading

To show the convergence of the SEM, three different discretized meshes are chosen for the same time step Δt = 0.01. Each mesh includes only two square elements (Figure 2) with a specific degree of Lagrange polynomials, n_ℓ.

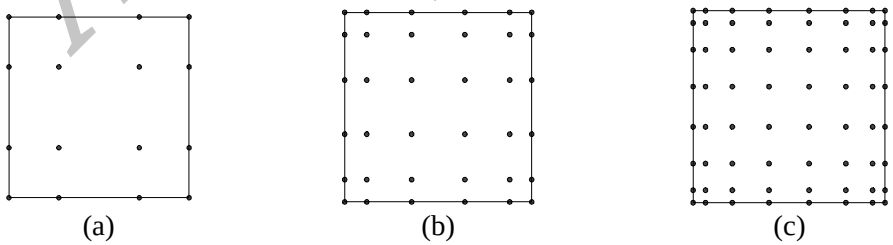

Figure 2. Various spectral elements with a certain degree of Lagrange polynomials: (a) n_ℓ = 3, (b) n_ℓ = 5, (c) n_ℓ = 7

The time histories of horizontal displacement at point A and horizontal stress at point B (see Figure 1a) are investigated. The numerical results by the SEM are compared with that of analytical solution. Figure 3 shows the horizontal displacement of point A, for the Heaviside step function loading. The results are depicted for three types of spectral elements inspected in this example. Also in this figure, the error distributions in the numerical results, i.e., the SEM solution-analytical solution, are shown. From this figure, one can see that all three types of spectral elements give very good results and that the higher-order elements give the better results.

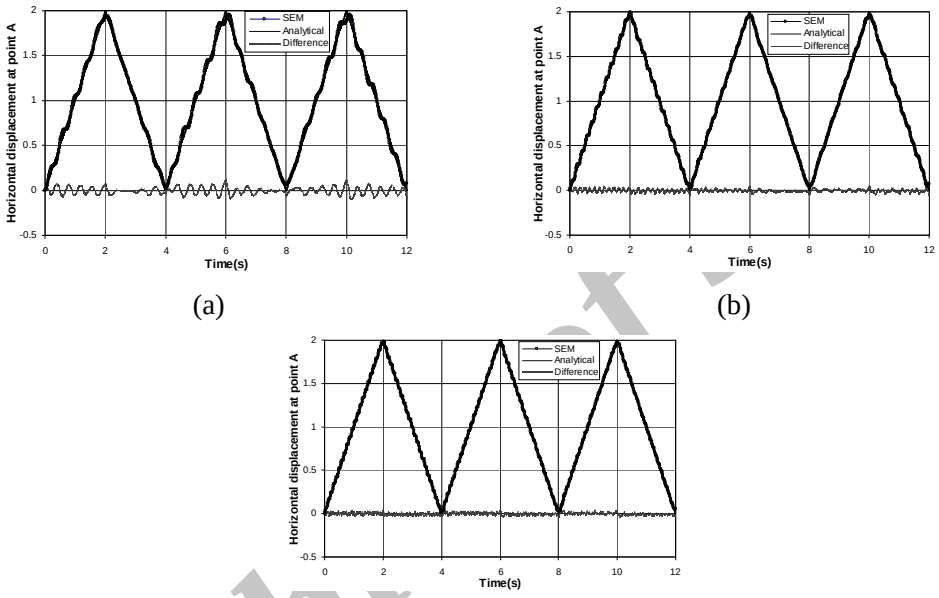

Figure 3. The SEM results of horizontal displacement at point A for three types of spectral elements with specified degrees of Lagrange polynomials, under Heaviside loading: (a) n_ℓ = 3, (b) n_ℓ = 5, (c) n_ℓ = 7

The horizontal stress histories at point B, for the Heaviside step function loading is shown in Figure 4. The results are drawn for three types of spectral elements. Good agreement between the SEM results and the analytical solution can be observed, especially with higher-order elements. The FEM results experience small oscillations around the analytical solutions at moments when the stress jumps. This type of oscillations are caused by the sudden application of the step load, and also observed in other numerical studies such as domain boundary element method [5], boundary element method [4], and hybrid BEM-FEM approach [21,22].

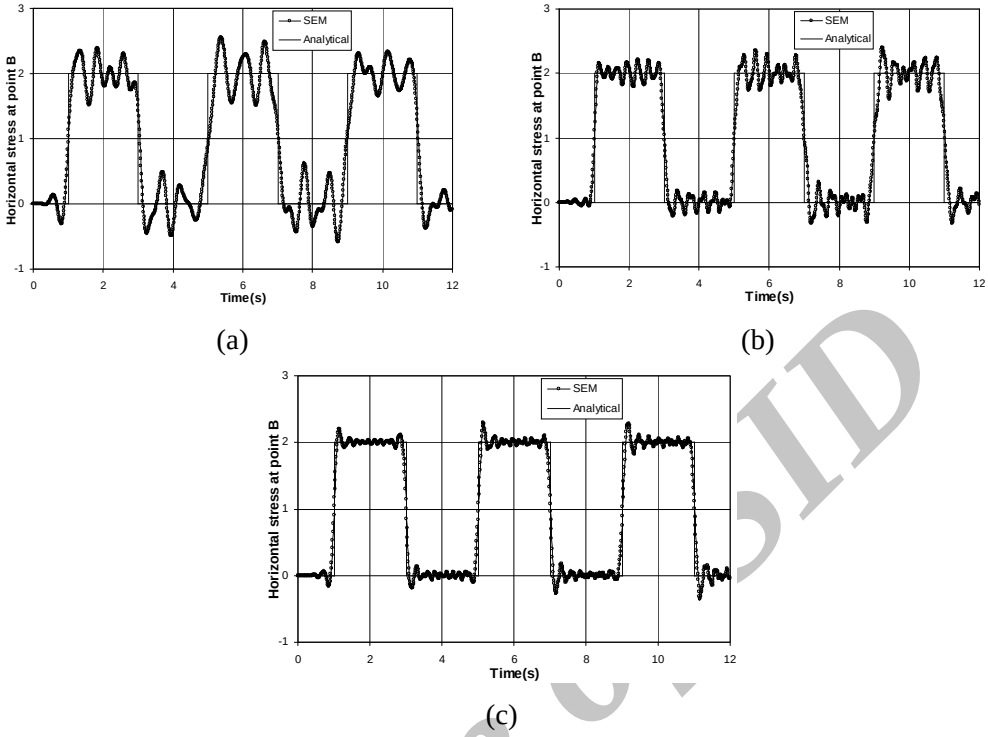

(a) (b)

(c)

Figure 4. The SEM results of horizontal stress at point B for three types of spectral elements with specified degrees of Lagrange polynomials, under Heaviside loading: (a) $n_\ell = 3$, (b) $n_\ell = 5$, (c) $n_\ell = 7$

Figure 5 shows the horizontal displacement of point A, for the triangular loading. The results are represented for three types of spectral elements examined in this example. As it is obvious from this figure, the results from the SEM and analytical approaches are almost identical. Excellent agreement can also be observed in the horizontal stress histories at point B as shown in Figure 6.

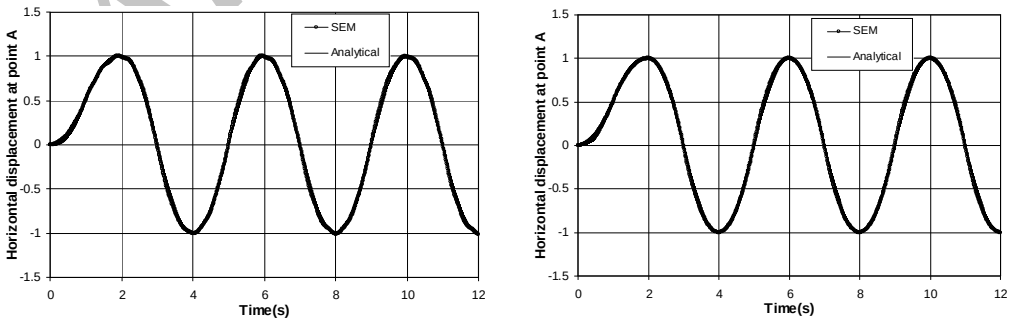

(a) (b)

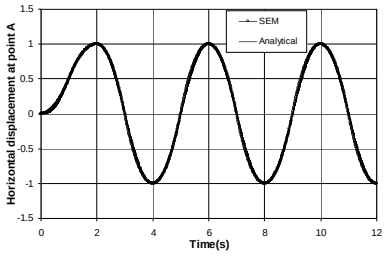

(c)

Figure 5. The SEM results of horizontal displacement at point A for three types of spectral elements with specified degrees of Lagrange polynomials, under triangular loading: (a) n_ℓ = 3, (b) n_ℓ = 5, (c) n_ℓ = 7

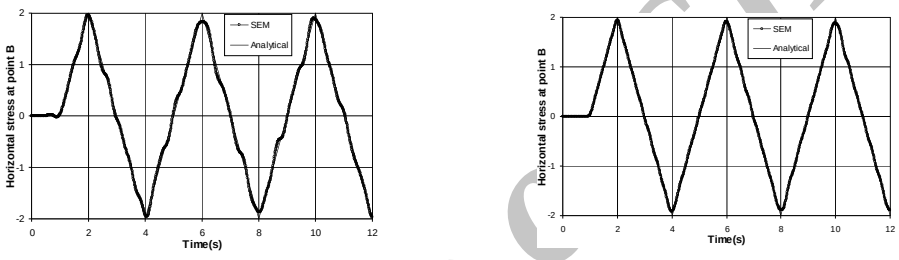

(a) (b)

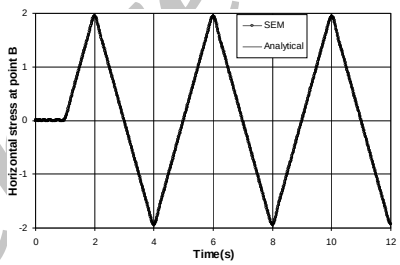

(c)

Figure 6. The SEM results of horizontal stress at point B for three types of spectral elements with specified degrees of Lagrange polynomials, under triangular loading: (a) n_ℓ = 3, (b) n_ℓ = 5, (c) n_ℓ = 7

5.2 Simply-supported beam subjected to concentrated loading

In this example, two-dimensional wave propagation problem of transverse vibration of beams is investigated to verify the proposed algorithm in comparison with analytical solution. A simply-supported beam, shown in Figure 7, is subjected to a concentrated mid-span Heaviside step function loading on its upper face. This loading has been introduced in Figure 1b. The material and geometrical properties of this example are as follows: the Young's modulus E=1, the Poisson's ratio ν = 0.3, the mass density ρ = 1, and the span

length, height, and width of the beam are 5, 1, and 1, respectively. With these material properties, primary and secondary wave propagation velocity are 1.1602 and 0.6202, respectively. Similar to the first example, three different discretized meshes are chosen for the same time step $\Delta t = 0.1$. Each mesh includes five square elements with a certain degree of Lagrange polynomials, n_ℓ.

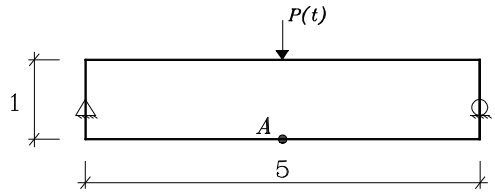

Figure 7. The second example. Geometry and boundary conditions of a simply-supported beam subjected to the mid-span concentrated loading of Heaviside step function type

The time histories of vertical displacement at point A (see Figure 7), obtained from the SEM approach and that of analytical method, are shown in Figure 8. The results are drawn for three types of spectral elements inspected in this example. Results of the two approaches agree very well. It is worthwhile remarking that the results shown in Figure 8 are pertaining to very coarse meshes in which few degrees of freedom are involved.

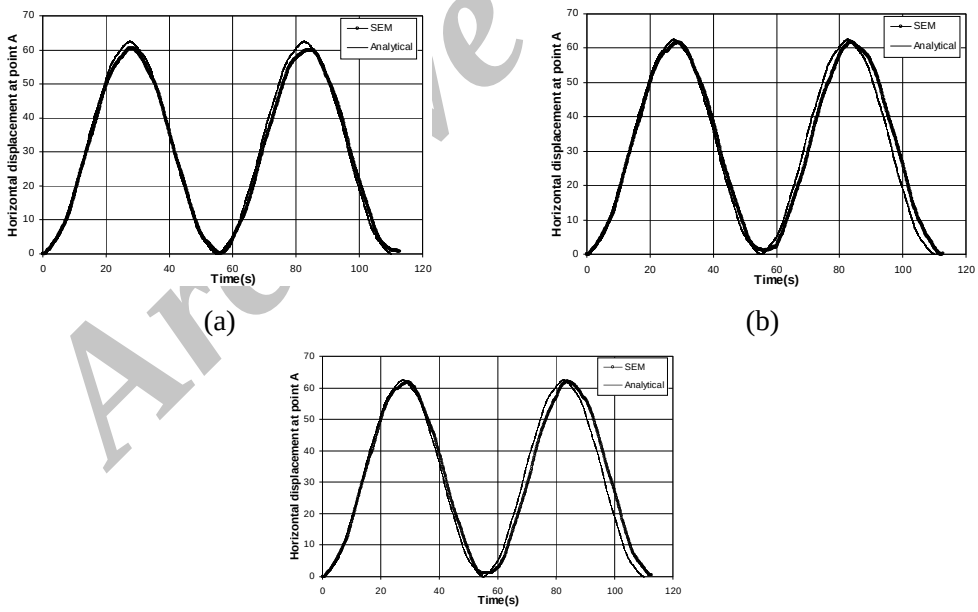

(a) (b)

(c)

Figure 8. The SEM results of vertical displacement at point A for three types of spectral elements with specified degrees of Lagrange polynomials: (a) $n_\ell = 2$, (b) $n_\ell = 4$, (c) $n_\ell = 6$ (the second example)

5.3 Rectangular bar subjected to longitudinal support motion

The longitudinal response of a rectangular bar caused by its support motion is examined in this example. The material properties of this example are as follows: the Young's modulus E=2×10^5, The Poisson's ratio v=0, and the mass density ρ=10. These material properties yield the maximum propagation velocity of stress waves c=141.42. This bar, whose length L=10 is twice its width W, is subjected to a longitudinal support motion at its left end, with traction free on its top, right, and bottom sides.

Assuming that the bar is initially at rest, the left support is subjected to horizontal translation of the Ricker type

$$u(t) = A_{\max}\left(1-2(\pi f_p(t-t_0))^2\right)\exp(-(\pi f_p(t-t_0))^2 \qquad (35)$$

where the predominant frequency f_p and the time shift parameter of the time history t_0 are selected to be 25 and 0.04, respectively. $A_{\max}$ denotes the maximum amplitude of the time history, which is chosen as 0.005.

Again, three different discretized meshes are chosen for the same time step Δt = 0.0005, and each mesh contains two square elements with a specific degree of Lagrange polynomials, n_ℓ. The time histories of horizontal displacement at point A (Figure 1a) are investigated. The numerical results by the SEM are compared with that of analytical solution as shown in Figure 9. The results are drawn for three types of spectral elements the same as the first example. From this figure, one can see that the higher-order elements give excellent results.

5.4 Plane portal frame subjected to lateral loading

In the fourth test, we consider a two-dimensional portal frame in order to demonstrate the accuracy of the SEM in modeling more realistic structures. As no analytical solution of this problem is available, comparison is made with the results based upon a meshless method [23], where they proposed a new method for solving transient elastodynamic problems based on the local boundary integral equation method and the moving least square approximation. We selected the same geometry (Figure 10a) and material properties as: $E\rho$ = 10000 and v = 0.2. The structure is fixed at the two bottom edges and is loaded by a lateral uniformly-distributed loading with ramp time dependence (Figure 10b). Similar to preceding examples, various meshes were inspected among which, the results concerning n_ℓ=2,4 and 6, are presented here. The mesh consists of five square elements whose boundaries are shown by dashed/solid lines in Figure 10a. We have selected the time step Δt = 0.005.

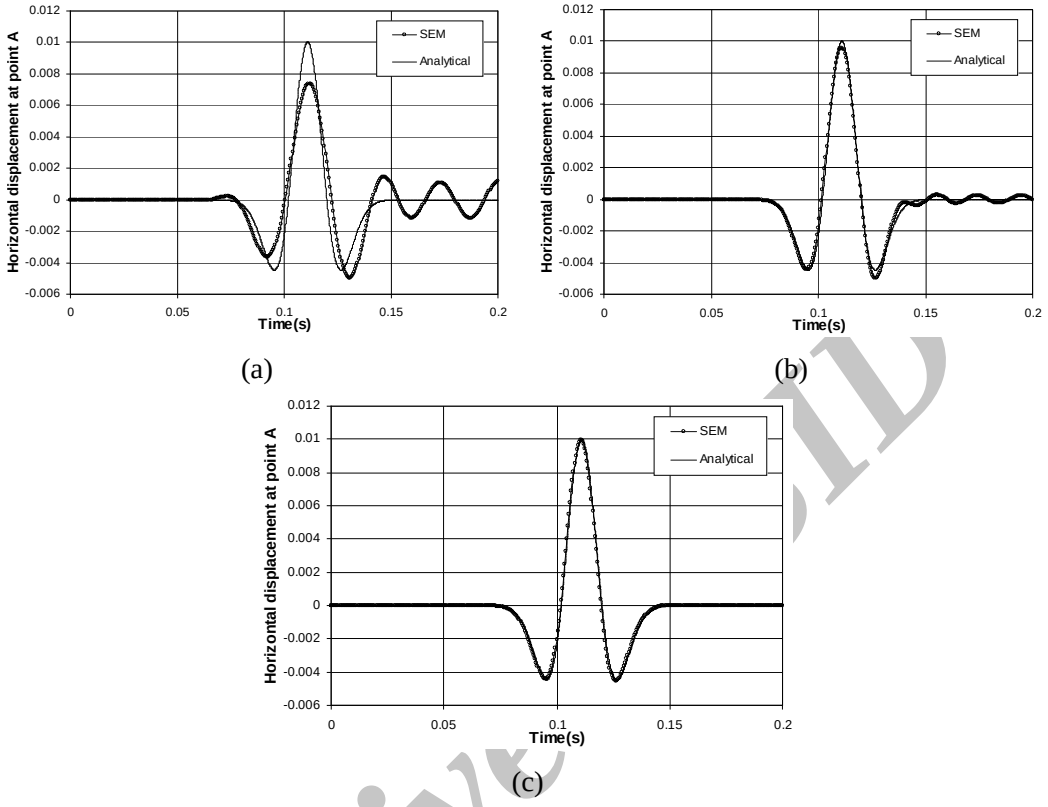

Figure 9. The SEM results of horizontal displacement at point A for three types of spectral elements with specific degrees of Lagrange polynomials: (a) $n_\ell = 4$, (b) $n_\ell = 6$, (c) $n_\ell = 8$ (the third example)

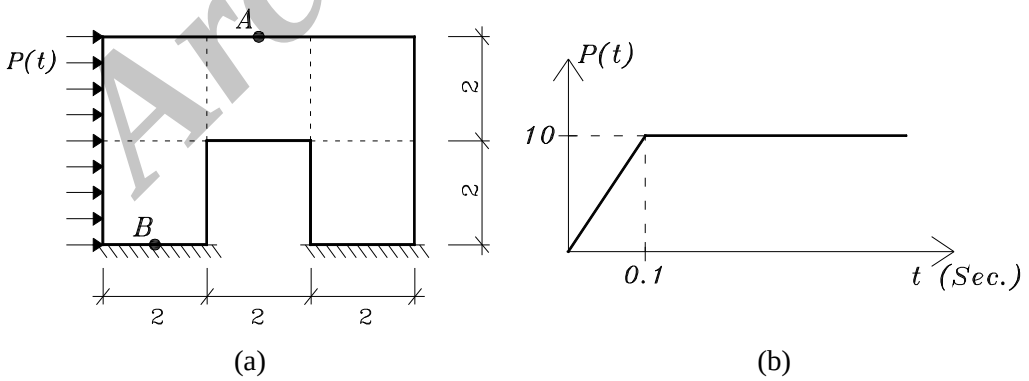

Figure 10. The fourth example. Portal frame subjected to lateral loading: (a) geometry and boundary conditions, (b) ramp time dependence function

The time variation of horizontal displacement at point A (Figure 10a) is shown in Figure 11a. The time variation of shear stress at point B (Figure 10a) is given in Figure 11b. All three meshes give almost converged time variations of numerical results. The results corresponding to higher order elements are identical to the results obtained by Sladek et al. [23] and are comparable with Figures 7 and 8 in [23].

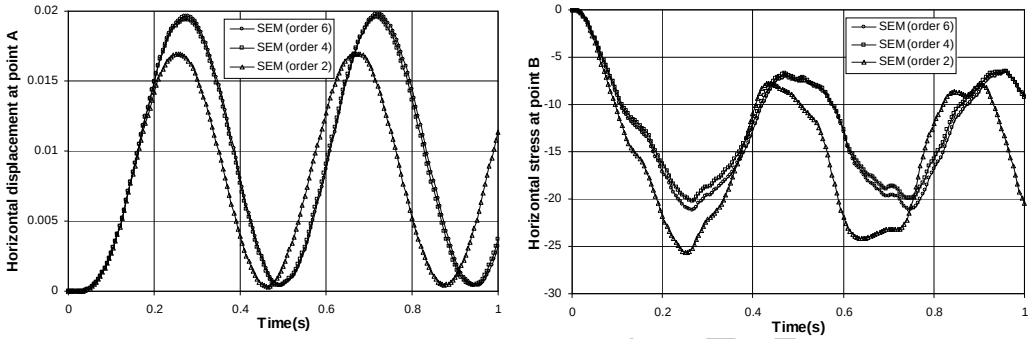

(a) (b)

Figure 11. The SEM results of the fourth example for three types (orders) of spectral elements with n_ℓ = 2, 4 and 6: (a) horizontal displacement at point A, (b) shear stress at point B

5.5 Bi-material rectangular bar subjected to impulsive loading

In the fifth and final example, we study a one-dimensional rectangular bar consisting of two different materials loaded by a sinusoidal impulsive loading, in order to check the accuracy of the SEM in analysis of impact problems. Solutions based upon a meshless Petrov-Galerkin formulation [24] are available for comparison. The segmented bar consists of two materials: one half is the steel and the other the aluminum (Figure 12a). This bar is fixed at its left end with traction free on its top and bottom sides. The right end side of bar is uniformly subjected to a tensile loading of sinusoidal pulse function (Figure 12b). The same geometry and loading function as in [24] are employed in this example as: $L = 2W = 50$ mm, and $P_0 = 100$ MPa. The material parameters are as follows: steel Young's modulus E_1 = 200 GPa, aluminum Young's modulus E_2=70GPa, ρ_1=7860 kg/m^3, ρ_2=2710 kg/m^3, and ν_1=ν_2= 0. These material properties yield the maximum propagation velocity of stress waves c_1=5044 m/s and c_2=5082 m/s.

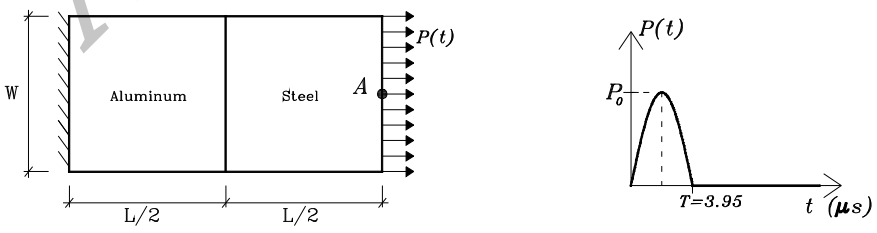

(a) (b)

Figure 12. The fifth example. Bi-material rectangular bar subjected to impulsive loading: (a) geometry and boundary conditions, (b) sinusoidal pulse loading.

To achieve convergence analysis of the SEM, three different discretized meshes are chosen for the same time step Δt = 0.05 μs. Each mesh contains two square elements with a certain degree of Lagrange polynomials, n_ℓ, in which, the results corresponding to n_ℓ = 2, 4 and 6, are represented.

The time histories of horizontal displacement at point A (see Figure 12a) are investigated. Figure 13 shows the horizontal displacement of point A, for three types of spectral elements examined in this example. Again, higher order meshes provide almost converged time variations of numerical results. The results corresponding to n_ℓ = 6 essentially coincide with the analytical solution presented by Batra et al. [24] and are virtually identical to the exact solutions of Figure 13 in [24].

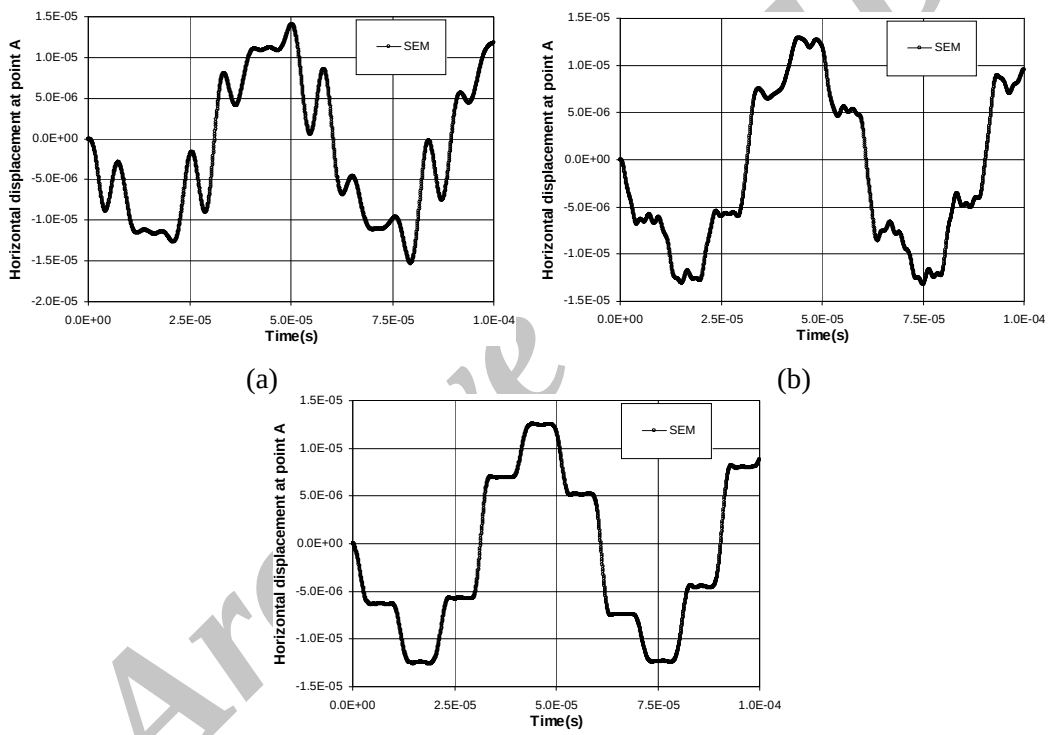

Figure 13. Horizontal displacement at point A concerning the fifth example, for three types of spectral elements with (a) n_ℓ = 2, (b) n_ℓ = 4, (c) n_ℓ = 6

Furthermore, in order to realize how time-step size affects the accuracy of the SEM approach, three different time-step sizes (Δt = 0.1, 0.2 and 0.3 μs) are chosen in the solution procedure. The results with the three time-step sizes by the SEM approach using the mesh of n_ℓ = 6 are also plotted together in Figure 14. Apparently, the smaller Δt is used, the better results are obtained. The results are consistent with the CFL condition of Eq. (34) in which,

simple calculations show that $\Delta t \leq 0.2$ μs are recommended.

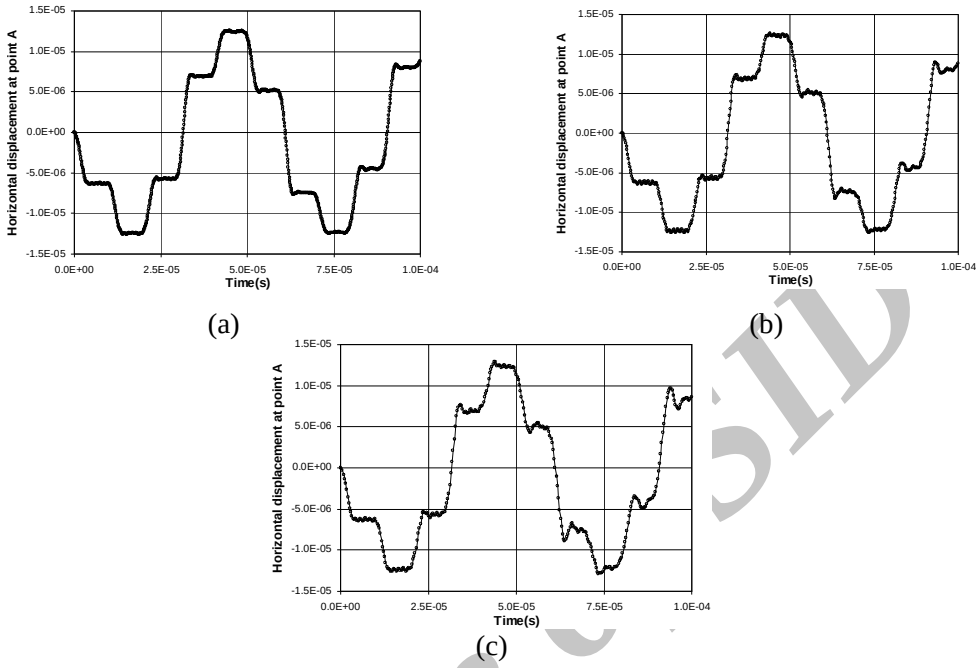

Figure 14. Comparison the SEM results of displacement at point A for (a) Δt = 0.1, (b) Δt = 0.2, (c) Δt = 0.3 μs

6. CONCLUSIONS

In this paper, detailed introduction of the spectral element method (SEM) for modeling wave propagation problems in time-domain has been presented. As would be realized from the detailed formulation to show a general picture of this method, the only difference between the SEM and the classical FEM could be summarized in two features: adoption of specific shape functions and numerical quadrature. Transient analyses of five examples have been successfully carried out using the SEM. In these examples, various dynamic behaviors, geometries, materials properties, boundary conditions, and transient load functions have been selected to illustrate the applicability and generality of this method. One may note that all these examples have been successfully modeled with very small number of DOFs, preserving very high accuracy comparing with other analytical and numerical solutions. As mentioned in the introduction, considering the applicability and generality of the SEM in wave propagation problems, development of this approach for other large-scale engineering seismology problems is currently followed by the authors [25].

Acknowledgements: A special gratitude to two anonymous reviewers, for their constructive advises that improved the manuscript. The authors wish to acknowledge the

financial support provided by the vice-chancellor of research affairs, Tarbiat Modares University.

REFERENCES

1. Sprague MA, Geers TL. A spectral-element method for modelling cavitation in transient fluid-structure interaction, *International Journal for Numerical Methods in Engineering*, **60**(2004) 2467-99.
2. Wegner JL, Yao MM, Zhang X. Dynamic wave-soil-structure interaction analysis in the time domain, *Computers and Structures*, **83**(2005) 2206-14.
3. Kole JS. Solving seismic wave propagation in elastic media using the matrix exponential approach, *Wave Motion*, **38** (2003) 279-93.
4. Carrer JAM, Mansur WJ. Time discontinuous linear traction approximation in time-domain BEM: 2-D elastodynamics, *International Journal for Numerical Methods in Engineering*, **49**(2000) 833-48.
5. Carrer JAM, Mansur WJ. Alternative time-marching schemes for elastodynamic analysis with the domain boundary element method formulation, *Computational Mechanics*, **34**(2004) 387-99.
6. Tanaka M, Chen W. Dual reciprocity BEM applied to transient elastodynamic problems with differential quadrature method in time, *Computer Methods in Applied Mechanics and Engineering*, **190**(2001) 2331-47.
7. Wang CC, Wang HC, Liou GS. Quadratic time domain BEM formulation for 2D elastodynamic transient analysis, *International Journal of Solids and Structures*, **34**(1997) 129-51.
8. Al-Khaleefi AM, Ali A, Rajakumar C, Kallivokas LF. Acoustic analysis with absorbing finite elements and far-field computations using free-space Green's functions, *Engineering Analysis with Boundary Elements*, **26**(2002) 929-37.
9. Givoli D, Hagstrom T, Patlashenko I. Finite element formulation with high-order absorbing boundary conditions for time-dependent waves, *Computer Methods in Applied Mechanics and Engineering*, **195**(2006) 3666-90.
10. Guddati MN, Tassoulas JL. Space-time finite elements for the analysis of transient wave propagation in unbounded layered media, *International Journal of Solids and Structures*, **36**(1999) 4699-723.
11. Kirby RM, Sherwin SJ. Stabilisation of spectral/hp element methods through spectral vanishing viscosity: Application to fluid mechanics modelling, *Computer Methods in Applied Mechanics and Engineering*, **195**(2006) 3128-44.
12. Chakraborty A, Gopalakrishnan S. A spectrally formulated finite element for wave propagation analysis in functionally graded beams, *International Journal of Solids and Structures*, **40**(2003) 2421-48.
13. Krawczuk M, Palacz M, Ostachowicz W. Wave propagation in plate structures for crack detection, *Finite Elements in Analysis and Design*, **40**(2004) 991-1004.
14. Kumar DS, Mahapatra DR, Gopalakrishnan S. A spectral finite element for wave propagation and structural diagnostic analysis of composite beam with transverse crack.

Finite Elements in Analysis and Design, **40**(2004) 1729-51.
15. Casadei F, Gabellini E, Fotia G, Maggio F, Quarteroni A. A mortar spectral/finite element method for complex 2D and 3D elastodynamic problems, *Computer Methods in Applied Mechanics and Engineering*, **191**(2002) 5119-48.
16. Komatitsch D, Vilotte J-P, Vai R, Castillo-Covarrubias JM, Sánchez-Sesma FJ. The spectral element method for elastic wave equations – application to 2-D and 3-D seismic problems, *International Journal for Numerical Methods in Engineering*, **45**(1999) 1139-64.
17. Zienkiewicz OC, Taylor RL. *The Finite Element Method*, Butterworth and Heinmann, 5th edition, Oxford, UK, 2000.
18. Seriani G, Priolo E. Spectral element method for acoustic wave simulation in heterogeneous media, *Finite Elements in Analysis and Design*, **16**(1994) 337-48.
19. Marfurt KJ. Accuracy of finite-difference and finite-element modeling of the scalar wave equation, *Geophysics*, **49**(1984) 533-49.
20. Timoshenko S, Young DH, Weaver W. *Vibration Problems in Engineering*, John Wiley and Sons, 4th edition, New York, USA, 1974.
21. Chien CC, Wu T.Y. A particular integral BEM/time-discontinuous FEM methodology for solving 2-D elastodynamic problems, *International Journal of Solids and Structures*, **38**(2001) 289-306.
22. Yu G, Mansur WJ, Carrer JAM, Lie ST. A more stable scheme for BEM/FEM coupling applied to two-dimensional elastodynamics, *Computers and Structures*, **79**(2001) 811-23.
23. Sladek J, Sladek V, Van Keer R. Meshless local boundary integral equation method for 2D elastodynamic problems, *International Journal for Numerical Methods in Engineering*, **57**(2003) 235-49.
24. Batra R.C, Porfiri M, Spinello D. Free and forced vibrations of a segmented bar by a meshless local Petrov–Galerkin (MLPG) formulation, *Computational Mechanics*, (2006) DOI 10.1007/s00466-006-0049-6.
25. Mirhashemian P, Khaji N, Shakib H. Soil-structure interaction (SSI) analysis using a hybrid spectral element/finite element (SE/FE) approach, *Soil Dynamics and Earthquake Engineering* (under review), 2009.